

Delocalization effects, entanglement entropy and spectral collapse of boson mixtures in a double well

F. Lingua¹, G. Mazzearella², V. Penna¹

¹ Dipartimento di Scienza Applicata e Tecnologia and U.d.R. CNISM, Politecnico di Torino, I-10129 Torino, Italy

² Dipartimento di Fisica e Astronomia Galileo Galilei and CNISM, Università di Padova, Via Marzolo 8, I-35131 Padova, Italy

E-mail: vittorio.penna@polito.it

Abstract. We investigate the ground-state properties of a two-species condensate of interacting bosons in a double-well potential. Each atomic species is described by a two-space-mode Bose-Hubbard model. The coupling of the two species is controlled by the interspecies interaction W . To analyze the ground state when W is varied in both the repulsive ($W > 0$) and the attractive ($W < 0$) regime, we apply two different approaches. First we solve the problem numerically i) to obtain an exact description of the ground-state structure and ii) to characterize its correlation properties by studying (the appropriate extensions to the present case of) the quantum Fisher information, the coherence visibility and the entanglement entropy as functions of W . Then we approach analytically the description of the low-energy scenario by means of the Bogoliubov scheme. In this framework the ground-state transition from delocalized to localized species (with space separation for $W > 0$, and mixing for $W < 0$) is well reproduced. These predictions are qualitatively corroborated by our numerical results. We show that such a transition features a spectral collapse reflecting the dramatic change of the dynamical algebra of the four-mode model Hamiltonian.

1. Introduction

Over the past decade, mixtures formed by two bosonic species have raised a considerable interest [1]-[7] due to the theoretic prediction of new exotic quantum phases. Such phases, determined by the competition of the interspecies interaction with the onsite interactions and tunneling amplitudes of each species, include, for example, unprecedented Mott-like states and types of superfluidity [1]-[3], and composite states exhibiting coexistence of different phases [6]. Mixtures, realized by means of either two atomic species [4] or the same species in two different internal states [5], have been trapped in optical lattices formed by many potential wells and are efficiently described in the Bose-Hubbard (BH) model framework [8, 9]. Their recent in-lab achievement has made stronger the interest for these systems.

The simplest but not trivial optical device where condensates of different atomic species can be loaded is the trap formed by a double-well potential. This has been realized by Albiez and co-workers [10] in 2005 by superposing a parabolic trap with a (sinusoidal) linear potential. This system has been widely explored within the mean-field approach to analyze the atomic counterpart of the Josephson effect in superconductor-oxide-superconductor junctions [11], the dynamical stability of binary mixtures [12, 13], different types of self-trapping solutions [14], the effectiveness of the space-mode description within the Gross-Pitaevskii picture [15, 16] and the Rabi-Josephson regime [17]. Further work has shown how the double-well system with two species can be exploited to model the dynamics of spin-orbit-coupled condensates [18, 19], to investigate their quantum evolution in the Raman-coupling regime [20] and energy-spectrum properties [21].

For several reasons, a fully-quantum analysis of few-well systems deserves a treatment too. First, because in the presence of sufficiently-low boson numbers only a BH-like formulation in terms of second-quantized space modes can provide a realistic description of microscopic processes in mixtures at essentially zero temperature. Second, because even the relatively simple models consisting of a mixture trapped in two wells feature complex dynamical behaviors owing to the strong nonlinearity of the interaction terms. This character affects, not only high-energy but also weakly-excited states including the ground state. Then, at very low temperatures, it is interesting to revisit nonlinear behaviors, first explored classically, in a fully-quantum environment. Finally, various well-established methods, both numerical and theoretical, seem to be applicable to study quantum models describing a mixture in two wells. Despite such circumstances, a rather small attention has been focused on quantum aspects of these systems [22]-[23].

This work aims to explore the low-energy properties of a two-species condensate confined in a double-well potential. The model describing this mixture is therefore a two-species Bose-Hubbard Hamiltonian defined on a two-site lattice (dimer) that, in addition to single-component interwell tunneling and onsite boson-boson interactions, also incorporates the density-density interaction W between atoms of different species. For brevity we call this model the two-species dimer (TSD).

The first aspect we consider is the numerical diagonalization of the TSD Hamiltonian in the zero-temperature regime. We find that, by keeping fixed the intraspecies interaction U , variations of interspecies interaction W produce significant changes in the structure of the ground state. On the repulsive side, increasing W drives the ground state from the uniform state (delocalization regime with mixed species) to a symmetric superposition of states exhibiting a macroscopic space separation (demixing) of the two species, passing through an intermediate configuration where the delocalized state and the symmetric demixed state coexist. When the interspecies interaction is attractive, instead, the uniform ground state “evolves” to a configuration in which atoms of different components tend to macroscopically populate the same well (localization regime with mixed species).

Studying appropriate extensions to the present case of the Fisher information [24, 25], the coherence visibility α [26, 27, 28] and the entanglement entropy S [29] in terms of interaction W allows us to characterize the ground state from the correlations point of view. In particular, we find that the maxima of α and S correspond to the on-set of a ground state in which a delocalized component and two symmetric localized states coexist. These numerical results improve our insight on how the ground-state structure depends on W .

The information obtained from the numerical determination of the ground-state configurations is then used to approach analytically the investigation of the low-energy regimes within the Bogoliubov approximation. In this framework we diagonalize the TSD Hamiltonian, in the strong-interaction ($|W| > U$) and in the weak-interaction ($|W| < U$) regime, by identifying weakly-occupied modes in the space-mode picture and in the momentum-mode picture, respectively. We reconstruct the low-energy spectrum, comparing the latter with the numerical eigenspectrum, and provide an approximate form of weakly-excited states. The demixing condition written in terms of the model parameters is derived analytically. We shed light on the spectral collapse occurring when the localization-delocalization transition of the species takes place, which causes the change of the energy spectrum from a discrete form to an almost continuous one [30]-[32]. The corresponding change of the algebraic structure of the Hamiltonian is also discussed.

2. The 2-species dimer Hamiltonian

We consider two interacting bosonic gases (denoted below by a and b) at zero temperature. Each species is confined in a three-dimensional trapping potential $V_{trap,c}(\mathbf{r})$ ($c = a, b$) achieved by superimposing an isotropic harmonic confinement in the transverse radial (x - y) plane and a symmetric double-well $V_{DW,c}(z)$ potential in the axial direction z . The resulting potential is $V_{trap,c}(\mathbf{r}) = m_c \omega_c^2 (x^2 + y^2)/2 + V_{DW,c}(z)$, where m_c is the boson mass of the c th component, ω_c the trapping frequency in the radial plane felt by the species c , and quantities $|m_a - m_b|$, $|\omega_a - \omega_b|$ are assumed to be sufficiently small. Due to the strong radial harmonic confinement we treat the system as quasi-

one-dimensional. Moreover, if the energy per particle in the axial direction is much smaller than the transverse level spacing $\hbar\omega_c$, then bosons can be assumed to stay in the ground state of the transverse harmonic oscillator. The model describing this system can be derived from the bosonic-field Hamiltonian by implementing the space-mode approximation (see, for example, [33, 34]). By expanding the field operators in the basis of the single-particle wave functions localized in each well, one achieves the two-species BH Hamiltonian

$$\hat{H} = \sum_{c=a,b} \hat{H}_c + \hat{H}_{ab} \quad (1)$$

with

$$\hat{H}_c = \frac{U_c}{2} \left[\hat{c}_L^\dagger \hat{c}_L^\dagger \hat{c}_L \hat{c}_L + \hat{c}_R^\dagger \hat{c}_R^\dagger \hat{c}_R \hat{c}_R \right] - J_c (\hat{c}_L^\dagger \hat{c}_R + \hat{c}_R^\dagger \hat{c}_L),$$

and

$$\hat{H}_{ab} = W (\hat{a}_L^\dagger \hat{a}_L \hat{b}_L^\dagger \hat{b}_L + \hat{a}_R^\dagger \hat{a}_R \hat{b}_R^\dagger \hat{b}_R) .$$

The operator $\hat{c}_v = \hat{a}_v(\hat{b}_v)$ annihilates a boson of species a (b) in the v th well ($v = L, R$, with L (R) representing the left (right) well), U_c is the amplitude of the intraspecies onsite interaction, J_c is the tunneling amplitude, and W is the interspecies interaction amplitude between bosons in the same well. Boson operators a_v , a_v^\dagger , b_v and b_v^\dagger , in addition to $[a_v, a_u^\dagger] = \delta_{uv} = [b_v, b_u^\dagger]$ with $u = L, R$, satisfy the commutators $[a_v, b_u] = 0$, and $[a_v, b_u^\dagger] = 0$. For each species, the total boson numbers \hat{N}_c commute with \hat{H} implying that $N_a = N_{aL} + N_{aR}$ and $N_b = N_{bL} + N_{bR}$ are conserved quantities. To further simplify the model we assume species a and b with the same mass, the same intraspecies s-wave scattering length, and experiencing identical double-well and harmonic confinements. In the following, we thus set $J_a = J_b \equiv J$ and $U_a = U_b \equiv U$, that is, the components a and b have the same hopping parameter and intraspecies interaction. We shall relax such assumptions whenever is possible.

3. Quantum analysis

We solve the eigenvalue equation associated to Hamiltonian (1)

$$\hat{H} |\psi\rangle_n = E_n |\psi\rangle_n \quad (2)$$

for fixed numbers N_a and N_b of bosons of species a and b , respectively. In this case the Hamiltonian can be represented by a $M \times M$ matrix with $M = (N_a + 1)(N_b + 1)$ in the basis $|i, j\rangle_L \otimes |N_a - i, N_b - j\rangle_R$ with $i \in [0, N_a]$ and $j \in [0, N_b]$. For each eigenvalue E_n , with $n = 1, 2, \dots, M$, the corresponding eigenstate $|\psi\rangle_n$ has the form

$$|\psi\rangle_n = \sum_{i=0}^{N_a} \sum_{j=0}^{N_b} C_n(i, j) |i, j\rangle_L |N_a - i, N_b - j\rangle_R, \quad (3)$$

where we assume –without loss of generality– that the coefficients $C_n(i, j)$ are real. In the ket $|i, j\rangle_L$, i (j) is the number of bosons of species a (b) in the left well, while in

$|N_a - i, N_b - j\rangle_R$, $N_a - i$ ($N_b - j$) is the number of bosons of species a (b) in the right well. Since we focus our attention on the ground state ($n = 1$), we simplify the notation by setting $C_1(i, j) \equiv C(i, j)$. When both the intra- and the interspecies interactions are zero, the ground state of Hamiltonian (1) is given by the product of two atomic (or $SU(2)$) coherent states (see, e. g., [35], [36])

$$|ACS\rangle = \frac{1}{\sqrt{N_a!N_b!}} \left(\frac{\hat{a}_L^\dagger + \hat{a}_R^\dagger}{\sqrt{2}} \right)^{N_a} \left(\frac{\hat{b}_L^\dagger + \hat{b}_R^\dagger}{\sqrt{2}} \right)^{N_b} |0, 0\rangle_L |0, 0\rangle_R, \quad (4)$$

where $|0, 0\rangle_L |0, 0\rangle_R$ is the state with no bosons. Coherent states of this form usually describe the superfluid phase for large J_c/U_c where bosons are uniformly distributed on the lattice and thus totally delocalized.

If one assumes that the intraspecies interactions U_a , U_b are essentially negligible with respect to the (absolute value of the) interspecies interaction $|W|$, the ground state of the TSD Hamiltonian is essentially formed by a symmetric superposition of two states with macroscopically populated wells. Its form depends on the sign of W . In particular, for $W > 0$ (repulsive interspecies interaction), the ground state has the form

$$|MPW\rangle \simeq \frac{1}{\sqrt{2}} \left(|N_a, 0\rangle_L |0, N_b\rangle_R + |0, N_b\rangle_L |N_a, 0\rangle_R \right), \quad (5)$$

whereas for $W < 0$ (attractive interspecies interaction) the ground state is

$$|MPW'\rangle \simeq \frac{1}{\sqrt{2}} \left(|N_a, N_b\rangle_L |0, 0\rangle_R + |0, 0\rangle_L |N_a, N_b\rangle_R \right). \quad (6)$$

In Figs. 1, 2 and 3, we show the ground state of Hamiltonian (1) when W is varied. The left panel of Fig. 1 represents the ground state when boson-boson interactions are zero, namely, $U = 0 = W$. This situation corresponds to the atomic coherent state (4). As shown in the right panel of the same figure for which $W = 0$ and $U = 0.1J$, the distribution $|C(i, j)|^2$ becomes narrower as soon as the on-site repulsive interaction is switched on. By keeping fixed $U = 0.1J$, a finite and repulsive interaction W balances

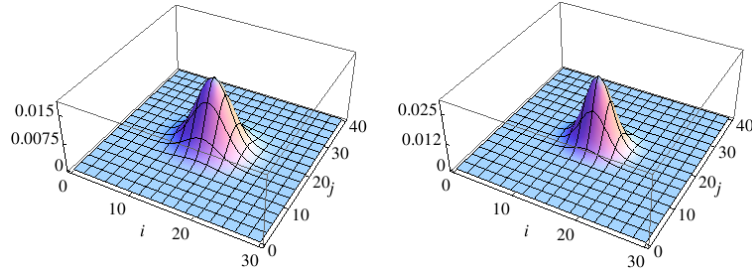


Figure 1. (Color online) Ground-state coefficients $|C(i, j)|^2$ vs i (left occupation numbers of species a) and j (left occupation number of species b) for $W = 0$, $U = 0$ (left panel), $U = 0.1$ (right panel) and boson numbers $N_a = 30$, $N_b = 40$. Energies in units of J .

this effect and causes the broadening of distribution $|C(i, j)|^2$ which becomes more and more pronounced when W is increased, as the left panel of the first row in Fig. 2 shows. By further increasing the interspecies repulsion, the ground-state structure

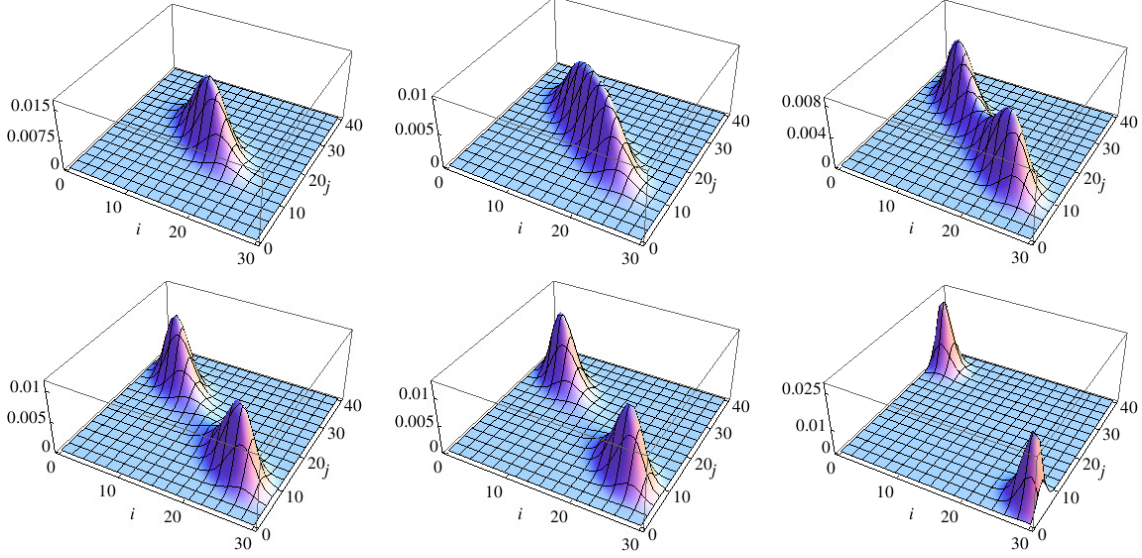


Figure 2. (Color online) Ground-state coefficients $|C(i, j)|^2$ vs i (left occupation numbers of species a) and j (left occupation number of species b) for $U = 0.1$. First row: $W = 0.15$, $W = 0.16$, $W = 0.165$. Second row: $W = 0.168$, $W = 0.17$, $W = 0.2$. Number of bosons: $N_a = 30$, $N_b = 40$. Energies in units of J .

exhibits a transition to a configuration characterized by the coexistence of a delocalized state (well represented by state (4)) and the two localized states $|N_a, 0\rangle_L |0, N_b\rangle_R$ and $|0, N_b\rangle_L |N_a, 0\rangle_R$. Such an effect (already observed for bosons in a three-well potential with ring geometry [37]) is well visible in the first row (right plot) of Fig. 2. This coexistence (where the ground state loses its coherence) is destroyed by a sufficiently-strong interspecies repulsion. In this case, the ground state becomes the symmetric superposition of (macroscopic) localized states described by state (5) and well illustrated in the second row (right plot) of Fig. 2. In correspondence to the same value of the onsite interaction U but with attractive interspecies interaction ($W < 0$, see Fig. 3), distribution of $|C(i, j)|^2$ displays the same changes characterizing the repulsive case when W is increased. Fig. 3 clearly shows that sufficiently strong interspecies attractions give rise to a superposition having the form of state (6) describing localized mixed species.

4. Ground-state correlation properties

We study the correlation properties of the ground state by following the same path followed in Ref. [38]. We thus use parameters that are appropriate extensions to the case under investigation of the Fisher information [24, 25], the coherence visibility [26, 27, 28]

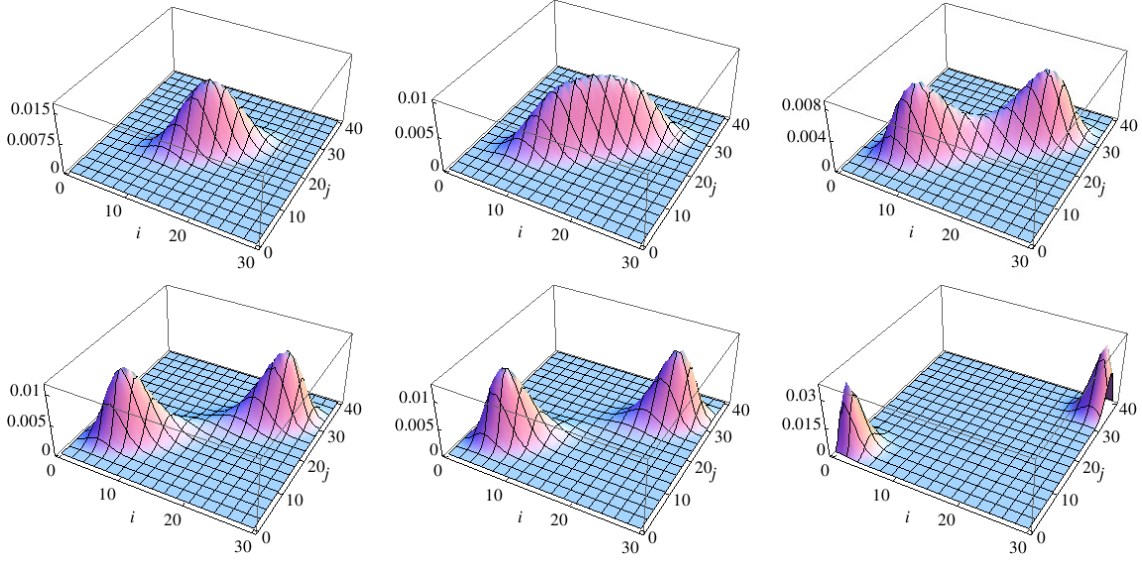


Figure 3. (Color online) Ground-state coefficients $|C(i, j)|^2$ vs i (left occupation number of species a) and j (left occupation number of species b) for $U = 0.1$. Top-bottom. First row: $W = -0.15$, $W = -0.16$, $W = -0.165$. Second row: $W = -0.168$, $W = -0.17$, $W = -0.21$. Boson numbers: $N_a = 30$, $N_b = 40$. Energies in units of J .

and the entanglement entropy [29]. The Fisher information is defined by

$$\mathcal{F} = \langle (\hat{N}_L - \hat{N}_R)^2 \rangle, \quad (7)$$

where the averages (here and in the following) are intended calculated with respect to the ground state, and $\hat{N}_v = \hat{a}_v^\dagger \hat{a}_v + \hat{b}_v^\dagger \hat{b}_v$ ($v = L, R$) is the boson number in the well v . The right-hand side of Eq. (7) provides a measure of the fluctuations of the interwell boson population imbalance due to the collective particle transfer caused by the tunneling of bosons across the central barrier. Note that the Fisher information is related to those entanglement properties descending from the quantum indistinguishability of the particles, a property known as multiparticle entanglement [25]. The quantity \mathcal{F} is equal to $(N_a + N_b)^2 = N^2$ when the ground state is state (6) and to $(N_a - N_b)^2 \equiv (\Delta N)^2$ in correspondence to state (5). Thus we use the indicator \mathcal{F} to have a feedback for the occurrence of symmetric superpositions of two states with macroscopically populated sites. We analyze the coherence properties of the ground state due to the single-particle hopping from the left well to the right one and back. To do this we use the following weighed coherence visibility

$$\alpha = \frac{N_a \alpha_a + N_b \alpha_b}{N_a + N_b} \quad (8)$$

$$\alpha_a = 2 \frac{\langle \hat{a}_L^\dagger \hat{a}_R \rangle}{N_a}, \quad \alpha_b = 2 \frac{\langle \hat{b}_L^\dagger \hat{b}_R \rangle}{N_b},$$

where α_c is the visibility (of the interference fringes in the ground-state momentum distribution) of the component c [26, 27, 28], [38]. In the spirit of the single-particle

tunneling, one can see, for example, from the first equation of the second row of Eq. (8), that the operator $\hat{a}_L^\dagger \hat{a}_R$ destroys a single boson in the right well and creates it in the left well. The coherence (8) is equal to one when the ground state is the state (4). Thus we use the indicator α to signal the emergence of the atomic coherent state. We study to what extent the ground state $|\psi\rangle$ (described by the density matrix $\hat{\rho} = |\psi\rangle\langle\psi|$) is affected by the genuine quantum correlations (entanglement) between the left well and the right one. We carry out this analysis from the bi-partition perspective with the two wells playing the role of the two partitions. Since the system is in a pure state, an excellent measure of the entanglement between the two wells is the entanglement entropy S . This quantity is obtained by first tracing out the degrees of freedom of the (right) left well from the density matrix $\hat{\rho}$ so as to get the reduced density matrix $\hat{\rho}_{L(R)}$, and, then, calculating the von Neumann entropy of the afore reduced density matrix by evaluating the trace of the matrix $-\hat{\rho}_{L(R)} \log_2 \hat{\rho}_{L(R)}$. The entanglement entropy for our systems is thus described by

$$S = -\hat{\rho}_{L(R)} \log_2 \hat{\rho}_{L(R)} = -\sum_{i=0}^{N_a} \sum_{j=0}^{N_b} |C_{i,j}|^2 \log_2 |C_{i,j}|^2, \quad (9)$$

where $C_{i,j}$ are the coefficients of the ground-state expansion in terms of Fock states [see Eq. (3)] that we determine numerically. The eventual maxima of S as a function of the boson-boson interaction will signal the ground states featuring the highest achievable degrees of left-right pure quantum correlations. As for the single-component case [44], these interactions might sign the onset of the self-trapping regime in the dynamics of the corresponding two-species bosonic Josephson junction. In Fig. 4 we have plotted the normalized Fisher information $F = \mathcal{F}/N^2$ (with \mathcal{F} given by Eq. (7)), the visibility α (see Eq. (8)), and entropy (9) as functions of interspecies interaction W by keeping U fixed. From this figure, we observe that F attains its maximum when the ground state has the shape of the superposition (6), see the right panel in the second row of Fig. 3, where $W/J = -0.21$.

The visibility α exhibits an interesting behavior heralded by the analysis displayed in Figs. 2 and 3. This shows that the ground state of Hamiltonian (1) is characterized by a high degree of coherence over a finite range of values of interaction W . The boundaries of this region are the two values of W signing the on-set of the coexistence of the delocalized state and the symmetric superposition of two localized states. In correspondence to such values of W , S features a double-peak structure characterized by two maxima, as shown by the bottom panel of Fig. 4. The von Neumann entropy thus confirms its effectiveness by measuring the increased degree of entanglement characterizing states (5) and (6).

5. Low-energy spectrum

The analysis of section 3 about the different regimes characterizing the ground state provides useful information for studying the spectrum of the model Hamiltonian through

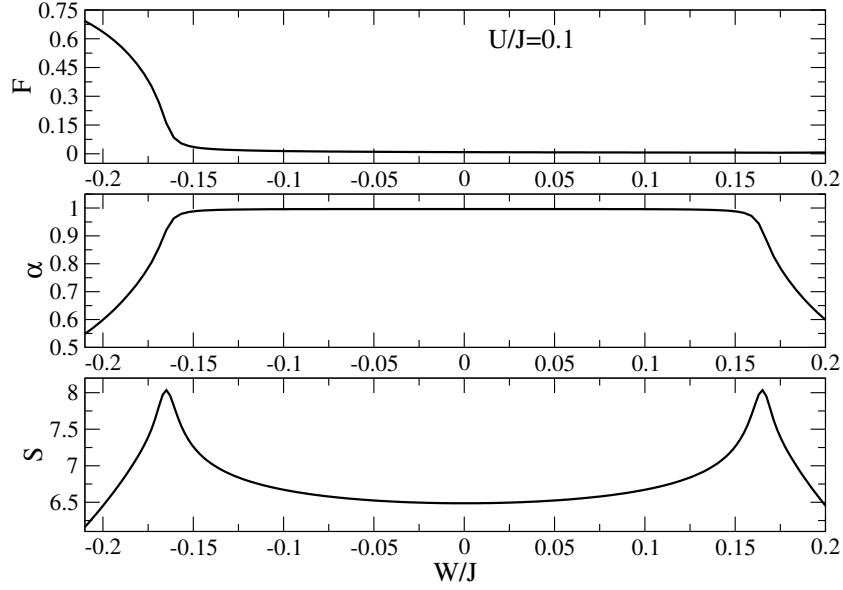


Figure 4. (Color online) Top panel: normalized Fisher information $F = \mathcal{F}/N^2$ (with \mathcal{F} given by Eq. (7)) vs W/J . Middle panel: coherence visibility α (see Eq. (8)) vs W/J . Bottom panel: entanglement entropy (9) vs W/J . In all three panels: $U/J = 0.1$. Number of bosons: $N_a = 30$, $N_b = 40$. All the quantities are dimensionless.

the Bogoliubov approach. For example, in the two strong-interaction regimes ($|W| > U_c$) relevant to $W > 0$ (repulsive interaction) and $W < 0$ (attractive interaction), the macroscopic localization effects illustrated in Figs. 2 and 3, respectively, show how for $W > 0$ one observes an almost complete separation of the two species strongly localized in different sites, whereas for $W < 0$ one has an almost complete merging of the two species localized at the same site. This allows one to identify weakly-occupied modes and thus to implement the Bogoliubov scheme.

A more complicated situation is found in the regimes $|W| < U_c$ (again including the cases $W < 0$ and $W > 0$), where the two bosonic species are completely delocalized and the boson populations essentially exhibit the same size in the two wells. In this second case, the correct approach for diagonalizing the Hamiltonian is found by looking for macroscopically-occupied modes within the momentum-mode picture.

5.1. Low-energy states with delocalized populations and spectral collapse

First we discuss the repulsive case of the two cases with $|W| < U_c$ involving delocalized populations and species mixing. Since the two species are almost equally distributed in the two wells a simple way to recognize weakly-occupied modes [30] is to introduce momentum-like operators $\hat{A} = (\hat{a}_L + \hat{a}_R)/\sqrt{2}$, $\hat{\alpha} = (\hat{a}_L - \hat{a}_R)/\sqrt{2}$, $\hat{B} = (\hat{b}_L + \hat{b}_R)/\sqrt{2}$

and $\hat{\beta} = (\hat{b}_L - \hat{b}_R)\sqrt{2}$. Note that the boson-number conservation is now given by

$$\begin{cases} N_a = N_{aR} + N_{aL} = N_A + N_\alpha, \\ N_b = N_{bR} + N_{bL} = N_B + N_\beta. \end{cases}$$

In the current regime ($|W| < U_c$), modes \hat{A} , \hat{B} are macroscopically occupied, ($N_A \gg N_\alpha$, $N_B \gg N_\beta$) and can be regarded as complex parameters within the Bogoliubov approximation. The application of this scheme (see [Appendix A](#)) provides the diagonal Hamiltonian

$$\hat{H}_D = K - 2J + \sqrt{R_\alpha} (2\hat{\alpha}^\dagger \hat{\alpha} + 1) + \sqrt{R_\beta} (2\hat{\beta}^\dagger \hat{\beta} + 1), \quad (10)$$

where $K = \sum_{c=a,b} U_c(N_c^2 - N_c)/4 + WN_aN_b/2 - JN$, and $J_a = J_b = J$ has been assumed. The symbols R_α and R_β are defined by

$$R_{\alpha,\beta} = J[J + (u \mp D)/4], \quad D = \sqrt{\Delta^2 + 4W^2N_aN_b},$$

with signs $- (+)$ corresponding to R_α (R_β), $u = U_aN_a + U_bN_b$, and $\Delta = U_aN_a - U_bN_b$. Note that, we have tacitly assumed $U_bN_b > U_aN_a$. In the opposite case $U_bN_b < U_aN_a$ the definitions of R_α , R_β are simply exchanged. The eigenvalues read

$$E(N_\alpha, N_\beta) = K - 2J + \sqrt{R_\alpha}(2N_\alpha + 1) + \sqrt{R_\beta}(2N_\beta + 1) \quad (11)$$

and the corresponding energy eigenstates

$$|E(N_\alpha, N_\beta)\rangle = |N_A\rangle|N_B\rangle\hat{U}^\dagger\hat{S}_\alpha\hat{S}_\beta|N_\alpha\rangle|N_\beta\rangle \quad (12)$$

are obtained by mixing the squeezed Fock states $\hat{S}_\alpha|N_\alpha\rangle$ and $\hat{S}_\beta|N_\beta\rangle$ (\hat{S}_α and \hat{S}_β are, in fact, squeezing operators) through the $SU(2)$ -group rotation \hat{U} . These states, \hat{U} and the $SU(1,1)$ -group transformations \hat{S}_α and \hat{S}_β are defined in [Appendix A](#).

As far as $4J + u > D$, the quantity R_α is positive and the contributions to the spectrum relevant to N_α and N_β are both discrete. A dramatic change in the energy spectrum emerges when $R_\alpha \rightarrow 0$. By rewriting the condition $4J + u > D$ in the form $U_aU_b + \Delta_J > W^2$, and observing that $\Delta_J = 8J(J+u)/N_aN_b \simeq 0$ for bosonic populations large enough, this effect takes place when

$$U_aU_b - W^2 \rightarrow 0^+. \quad (13)$$

The latter formula reproduces for $U_a = U_b = U$ (twin species) the well-known mixing condition $U = W$ characterizing bosonic mixtures and derived heuristically in Ref. [\[39\]](#) for large-size lattices. For W^2 approaching U_aU_b from below, the interlevel separation for the α -mode spectrum tends to vanish thus determining, for $W^2 = U_aU_b$, the transition to a continuous spectrum. Hamiltonian [\(A.1\)](#) (emerging from the Bogoliubov approach and leading to the diagonal form [\(10\)](#)) thus predicts a *spectral collapse* of the energy

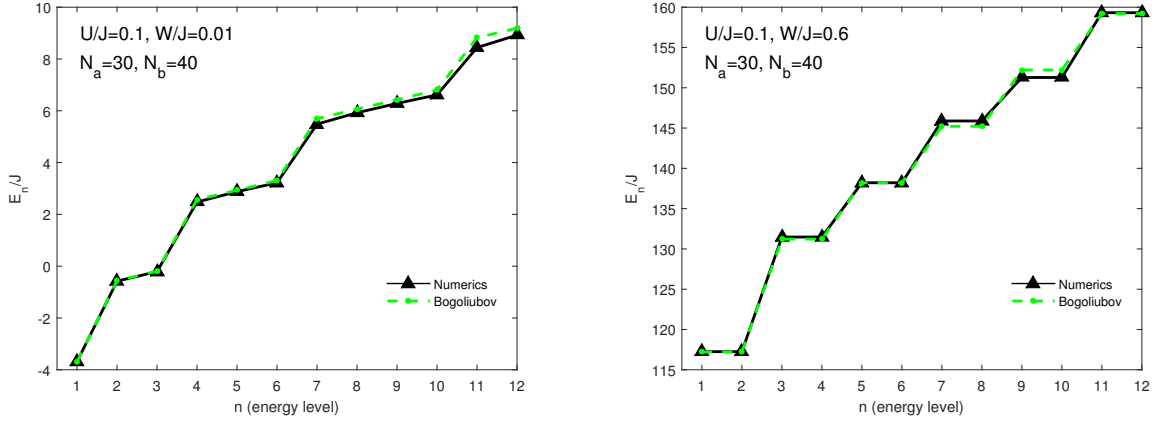


Figure 5. (Color online) Case $W > 0$ with $U_a = U_b \equiv U$. Left panel: $W < U$. Black triangles: eigenvalues obtained numerically. Green dots: Eigenvalues obtained by Eq. (11), $(N_\alpha, N_\beta) = (0, 0), (1, 0), (0, 1), (1, 1), (2, 1), \dots$ correspond to the energy level $n = 1, 2, 3, 4, 5, \dots$ ($n = 1$ denotes the ground state). Right panel: $W > U$. Black triangles: eigenvalues obtained numerically. Green dots: Eigenvalues obtained by Eq. (14), $(N_{aR}, N_{bL}) = (0, 0), (0, 1), (1, 0), (1, 1), (1, 2), \dots$ correspond to the energy level $n = 1, 2, 3, 4, 5, \dots$. All the quantities are dimensionless. Lines are for eye-guide.

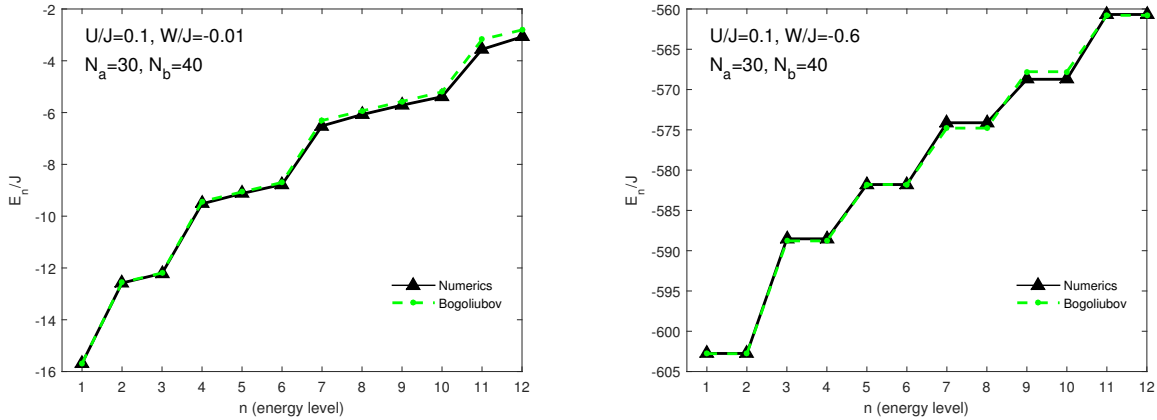


Figure 6. (Color online) Case $W < 0$ with $U_a = U_b \equiv U$. Left panel: $|W| < U$. Black triangles: eigenvalues obtained numerically. Green dots: Eigenvalues obtained by Eq. (11), $(N_\alpha, N_\beta) = (0, 0), (1, 0), (0, 1), (1, 1), (2, 1), \dots$ correspond to the energy level $n = 1, 2, 3, 4, 5, \dots$ ($n = 1$ denotes the ground state). Right panel: $|W| > U$. Black triangles: eigenvalues obtained numerically. Green dots: Eigenvalues obtained by Eq. (C.1), $(N_{aR}, N_{bR}) = (0, 0), (0, 1), (1, 0), (1, 1), (1, 2), \dots$ correspond to the energy level $n = 1, 2, 3, 4, 5, \dots$. All the quantities are dimensionless. Lines are for eye-guide.

levels for $W^2 \rightarrow U_a U_b$. This mechanism is discussed in detail in [30] and [31]. The resulting macroscopic effect (also observed in Ref. ([32])) can be interpreted as the hallmark of the transition from the mixed-species regime (illustrated in the first row, left panel of Fig. 2) to the demixed regime involving, for $W > 0$, the spatial separation

of the two species (illustrated in the second row, right panel of Fig. 2).

The left panels of Figures 5 and 6 corresponding to the repulsive and the attractive case, respectively, describe the eigenvalues of the 2-species Hamiltonian in the weak-interaction regime $|W| < U$. Such figures clearly show the excellent agreement between the eigenvalues provided by equation (11) and the eigenvalues determined numerically. By following the same “Bogoliubov vs numerics” path, it is interesting to check if the expected transition to a continuous spectrum (spectral collapse) discussed above, is observed. To this end we have calculated the exact eigenvalues of model (1) for two cases described in Fig. 7 by the squares-solid (red) line ($W \ll U$) and circles-dashed (black) line where the interspecies interaction $W \simeq U$. The latter case represents the limit $U_a U_b - W^2 \rightarrow 0^+$ with $U_a = U_b = U$ (see formula (13)). The comparison of the two lines clearly shows how the continuous character of the energy spectrum emerges in the limit $U - W \rightarrow 0^+$.

The change $W > 0 \rightarrow W < 0$ does not affect the essence of the previous scheme so that the same conclusions can be found, in the attractive case, when $|W|$ is increased and the demixing effect illustrated in Fig. 3 takes place. The dramatic change of the algebraic structure of \hat{H} reflecting the occurrence of the spectral collapse suggests that a different mode picture must be used when $|W| > U$ in order to get the Hamiltonian into the diagonal form. This is discussed in the next subsection.

5.2. Low-energy states with localized populations

Repulsive interaction. For W sufficiently larger than U_c the boson distributions feature two possible forms

$$\begin{cases} N_{aR} \ll N_{aL} \simeq N_a, & N_{bL} \ll N_{bR} \simeq N_b, \\ N_{bR} \ll N_{bL} \simeq N_b, & N_{aL} \ll N_{aR} \simeq N_a, \end{cases}$$

where two bosonic modes are macroscopically occupied and $N_c = N_{cL} + N_{cR}$ with $c = a, b$ are conserved quantities. Such configurations are totally equivalent under the exchange, for each species, of the left and right populations. The application of the Bogoliubov scheme is discussed in Appendix B for the case $N_{aR} \ll N_a$ and $N_{bL} \ll N_b$. For this configuration the eigenvalues of \hat{H} are found to be

$$E_1(N_{aR}, N_{bL}) \simeq E_0(N_a, N_b) + \sigma_a N_{aR} + \sigma_b N_{bL}, \quad (14)$$

with

$$E_0(N_a, N_b) = \sum_{c=a,b} \left[\frac{U_c}{2} (N_c^2 - N_c) - \frac{J_c^2 N_c}{\sigma_c} \right], \quad (15)$$

and

$$\sigma_a = W N_b - U_a N_a, \quad \sigma_b = W N_a - U_b N_b. \quad (16)$$

Note that the general conditions $U_a \neq U_b$ and $J_a \neq J_b$ have been kept since they do not affect the diagonalization process. The eigenvalues of the 2-species Hamiltonian in

the strong-interaction regime $|W| > U$ are illustrated in the right panel of Figure 5 in the repulsive case. Also in this case, the eigenvalues provided by equation (14) and the eigenvalues determined numerically show an excellent agreement. The corresponding eigenstates are

$$|E_1(N_{bL}, N_{aR})\rangle = |N_{aL}\rangle |z_{bL}, N_{bL}\rangle |z_{aR}, N_{aR}\rangle |N_{bR}\rangle \quad (17)$$

(recall that $N_{bR} = N_b - N_{bL}$ and $N_{aL} = N_a - N_{aR}$) where the two generalized Glauber coherent states [40]

$$|z_{bL}, N_{bL}\rangle = \hat{D}(z_{bL})|N_{bL}\rangle, \quad |z_{aR}, N_{aR}\rangle = \hat{D}(z_{aR})|N_{aR}\rangle$$

incorporate the displacement operators $\hat{D}(z_{aR})$ and $\hat{D}(z_{bL})$. The latter ensure the reduction of Hamiltonian \hat{H} to the diagonal form for $z_{aR} \equiv J_a \sqrt{N_a}/\sigma_a$, and $z_{bL} \equiv J_b \sqrt{N_b}/\sigma_b$. Operators $\hat{D}(z_{aR})$ and $\hat{D}(z_{bL})$ are defined in Appendix B. Formula (14) shows that the lowest energy state of the double-well system is found for $N_{bL} = N_{aR} = 0$ which gives

$$|E_1(0, 0)\rangle = |N_a\rangle |z_{bL}\rangle |z_{aR}\rangle |N_b\rangle.$$

In this case $|z_{bL}, N_{bL}\rangle$ and $|z_{aR}, N_{aR}\rangle$ reduce to two Glauber coherent states $|z_{bL}\rangle$ and $|z_{aR}\rangle$ implying that the minimum-uncertainty relation of boson operators reaches its optimized form in the ground state (see Appendix B).

The same diagonalization scheme can be applied to the case $N_{aL} \ll N_{aR}$, $N_{bR} \ll N_{bL}$ and implies the approximation $H \simeq H_2$ described by formula (B.2). The eigenvalues and the eigenstates of \hat{H}_2 are found to be

$$E_2(N_{aL}, N_{bR}) \simeq E_0(N_a, N_b) + \sigma_a N_{aL} + \sigma_b N_{bR}, \quad (18)$$

$$|E_2(N_{aL}, N_{bR})\rangle = |z_{aL}, N_{aL}\rangle |N_{bL}\rangle |N_{aR}\rangle |z_{bR}, N_{bR}\rangle,$$

and, following the same lines leading to equations (B.3), one determines the conditions $z_{aL} \equiv J_a \sqrt{N_a}/\sigma_a$, and $z_{bR} \equiv J_b \sqrt{N_b}/\sigma_b$ taking the Hamiltonian into the diagonal form. For $N_{aL} = N_{bR} = 0$ the lowest energy eigenvalue is achieved which satisfies $E_2(0, 0) = E_0(N_a, N_b) \equiv E_1(0, 0)$ and is associated with $|E_2(0, 0)\rangle = |z_{aL}\rangle |N_a\rangle |N_b\rangle |z_{bR}\rangle$ again containing two Glauber coherent states. Due to the degeneracy of the Bogoliubov spectrum (eigenvalues (14) and (18) are identical), the obvious form of the ground state (gs) is thus given by

$$|E_{gs}\rangle = \frac{1}{\sqrt{2}} \left(|E_1(0, 0)\rangle + |E_2(0, 0)\rangle \right),$$

which well reproduces qualitatively the behavior of the ground state illustrated in the second row of Fig. 2 for W sufficiently larger than U . Weakly-excited states can be derived together with their eigenvalues by constructing suitable symmetrized combinations of equal-energy states $|E_{\pm}(q, p)\rangle = (|E_1(q, p)\rangle \pm |E_2(p, q)\rangle)/\sqrt{2}$ where $N_{aR} = N_{aL} = q$ and $N_{bR} = N_{bL} = p$. The degeneracy characterizing such states, well known for a system of two symmetric wells with a single atomic species [34], can be removed by applying to states $|E_{\pm}(q, p)\rangle$ the approximation scheme developed in reference [41] for a double-well potential.

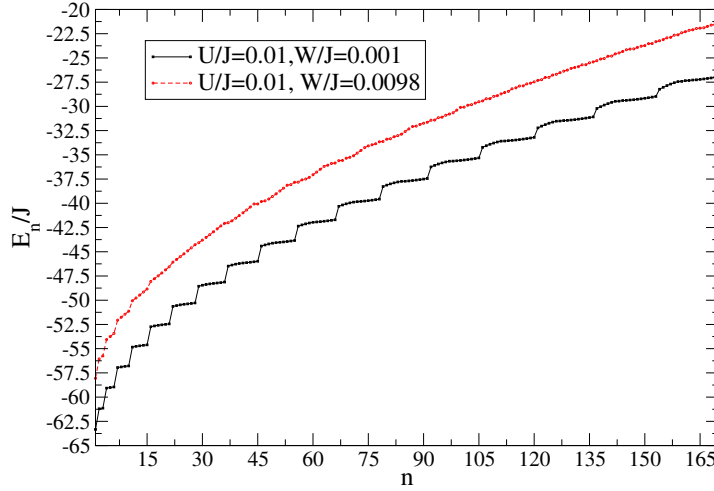


Figure 7. (Color online) Numerical calculation of the energy levels of model (1). $N_a = 30$, $N_b = 40$, $U_a/J = U_b/J \equiv U/J = 0.01$. The spectral collapse is illustrated by comparing the spectrum for $W/J = 0.001$ (squares-solid) and $W/J = 0.0098$ (circle-dashed). Horizontal axis: Excitation number n . Vertical axis: eigenvalues E_n of Hamiltonian (1) in units of J .

Attractive interaction. In the strong-interaction regime, namely for $|W|$ sufficiently larger than U , the two configurations

$$\begin{cases} N_{aR} \ll N_{aL} \simeq N_a, & N_{bR} \ll N_{bL} \simeq N_b, \\ N_{aL} \ll N_{aR} \simeq N_a, & N_{bL} \ll N_{bR} \simeq N_b, \end{cases}$$

—both entailing the localization of the two species in one of the two wells— describe the ground state. Due to the attractive interaction the macroscopically occupied modes are those corresponding to the same well for each population. The diagonal Hamiltonian of this case features the eigenvalues

$$E_3(N_{aR}, N_{bR}) \simeq \tilde{E}_0(N_a, N_b) + \sigma_a N_{aR} + \sigma_b N_{aL}, \quad (19)$$

derived in [Appendix C](#). The equivalent spectrum found by exchanging left and right populations is given by formula (C.2). The right panel of Figure 6 illustrates the Bogoliubov spectrum (19) and the numerical spectrum for the TDS model in the strong-interaction attractive case $|W| > U$. As in the repulsive case, an excellent agreement characterizes, at low energies, the Bogoliubov and numerical eigenvalues.

Concluding remarks. To better illustrate the range of validity of the Bogoliubov scheme, we compare the Bogoliubov and the numerical spectrum for a number of energy levels ($n = 40$) larger than that of Figs. 5 and 6. Fig. 8 shows that their agreement remains qualitatively satisfactory when n is increased. Both the case $W < U$ (left panel) and $W > U$ (right panel) are considered for $W > 0$. The same results can be shown to hold in the attractive case. For $|W| > U$ and large number of bosons, the

agreement between the exact numerical diagonalization and the Bogoliubov scheme can be estimated by calculating the relative error as a function of parameters σ_a and σ_b . This is defined by

$$\Delta E_n = \left[\frac{\sum_n (E_n - E_{n,B})^2}{\sum_n E_n^2} \right]^{1/2}, \quad (20)$$

where E_n and $E_{n,B}$ refer to the levels obtained numerically and from the Bogoliubov spectrum (14), respectively. Fig. 9 shows the dependence of ΔE_n from σ_a and σ_b at fixed $W > 0$ and U . σ_a and σ_b can be varied by increasing the boson number N since $\sigma_a = (3W - 2U)N/5$ and $\sigma_b = (2W - 3U)N/5$ with a fixed population ratio $N_a/N_b = 2/3$ (see (16)). The rapid decreasing of ΔE_n for large N (in Fig. 9, $\sigma_a = 8$, $\sigma_b = 1$ correspond to $N = 130$) highlights that, in the semiclassical limit, the Bogoliubov spectrum approaches the numerical one (the same results are found in the attractive case $W < 0$). The only *caveat* in applying the Bogoliubov scheme concerns the ratio N_a/N_b and U/W . A careful choice of the latter quantities must be done in order to avoid possible diverging behavior of the constant energy (15). This pathology does not affect the Bogoliubov spectrum found in section (5.1) for $|W| < U$.

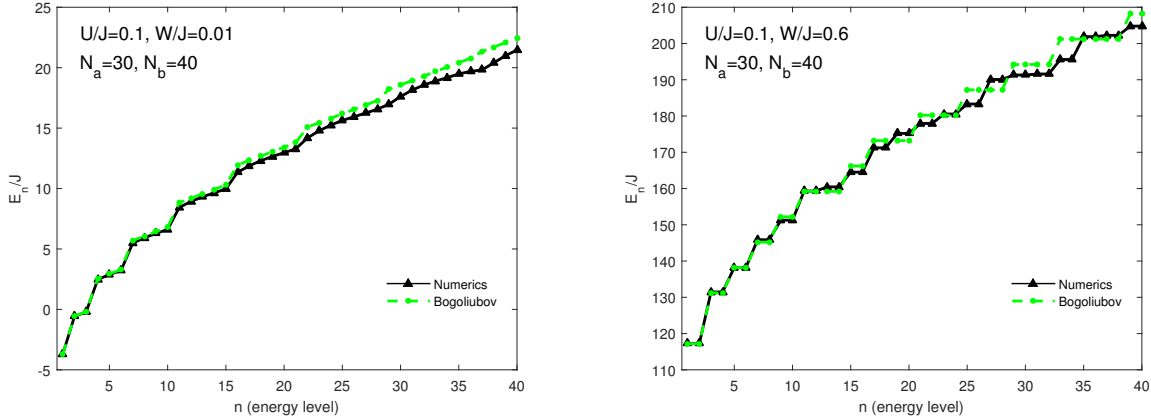


Figure 8. (Color online) In these panels we show that the agreement of the Bogoliubov and the numerical spectrum remains satisfactory even for a larger number of energy levels. Deviations become more and more visible for n larger than $n \sim 30$. Both the case $W < U$ (left panel) and $W > U$ (right panel) are considered for $W > 0$.

6. Conclusions

We have studied a bosonic binary mixture confined by a one-dimensional double-well potential (TSD model) where each atomic species is described by a BH model and the two species are coupled via an onsite density-density interaction W . We have investigated the system by adopting two different approaches and analyzed the ground state by varying W in both the repulsive ($W > 0$) and the attractive ($W < 0$) case.

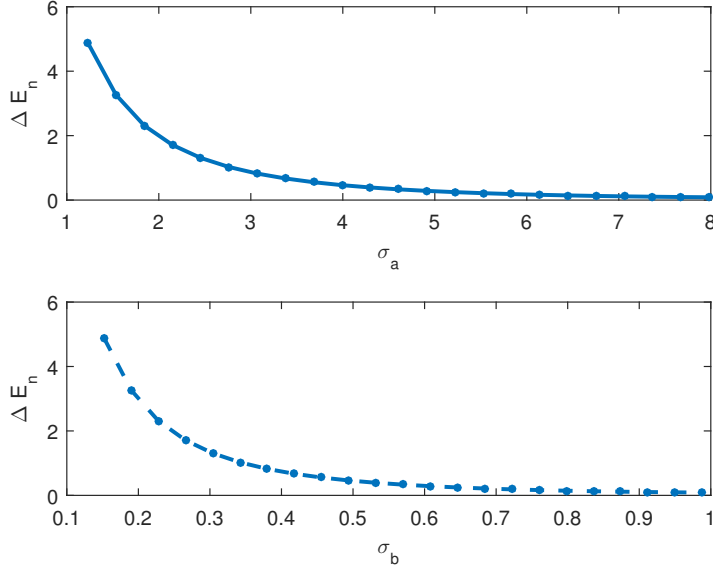


Figure 9. (Color online) Relative error ΔE_n , described by formula (20), as a function of σ_a (upper panel) and σ_b (lower panel), for $W = 0.169$, and $U = 0.1$ (see eq. (16)). Both σ_a and σ_b are varied increasing N with $N_a/N_b = 0.66$. The two panels show how the Bogoliubov spectrum approaches the numerical spectrum in the limit $N \gg 1$.

First, we have diagonalized numerically the TSD model and obtained an exact description of the ground-state structure. Then, we have characterized the TSD lowest energy state from the viewpoint of correlation properties. In this respect, we have studied (the appropriate specializations to the case under study of) the quantum Fisher information, the coherence visibility and the entanglement entropy as functions of W , showing their sensitivity to the changes of the ground-state structure.

As a second, after identifying the weakly-occupied bosonic modes in the four regimes characterized by W (interspecies interaction) and U_c (onsite interaction of species $c = a, b$), we have reconstructed within the Bogoliubov approach the energy spectrum and the relevant low-energy states. The low-energy part of the spectrum displays an excellent agreement with the spectrum calculated numerically. This agreement is shown to improve when the total boson number N is increased. Finally, we have shown how moving from the delocalized regime to the localized one –where both species feature macroscopic components, separated ($W > 0$) or mixed ($W < 0$)– determines a spectral collapse in which the interlevel distance became smaller and smaller when W^2 approaches $U_a U_b$ from below. The eigenstates, exhibiting squeezed-state components for $U_a U_b > W^2$, assume a form characterized by Glauber-state components for $W^2 > U_a U_b$, reflecting the new algebraic structure of the Hamiltonian in this regime.

Acknowledgments

The authors acknowledge the Ministero dell'Istruzione, Università e Ricerca, (MIUR) for the support provided by the Grant PRIN 2010LLKJBX.

Appendix A. Reduction of \hat{H} to a diagonal form in the regime $|W| < U_c$

Within the Bogoliubov scheme, operators \hat{A} , \hat{B} can be seen as complex parameters if $N_a \gg N_\alpha$ and $N_b \gg N_\beta$. With the substitutions $\hat{A} \rightarrow e^{i\phi_A} \sqrt{N_a}$, $\hat{B} \rightarrow e^{i\phi_B} \sqrt{N_b}$ (in which the phase factors associated to \hat{A} and \hat{B} can be removed due to the U(1) symmetry of the Hamiltonian) model (1) reduces to

$$\begin{aligned} \hat{H} = & \frac{W}{2} \sqrt{N_a N_b} (\hat{\alpha} + \hat{\alpha}^\dagger) (\hat{\beta} + \hat{\beta}^\dagger) + 2J_a \hat{N}_\alpha + 2J_b \hat{N}_\beta \\ & + \frac{U_a}{4} N_a (\hat{\alpha} + \hat{\alpha}^\dagger)^2 + \frac{U_b}{4} N_b (\hat{\beta} + \hat{\beta}^\dagger)^2 + K, \end{aligned} \quad (\text{A.1})$$

where the terms depending on N_a , N_b are grouped in the constant

$$K = \frac{U_a}{4} (N_a^2 - N_a) + \frac{U_b}{4} (N_b^2 - N_b) + \frac{W}{2} N_a N_b - JN,$$

and third-order (or higher-order) terms have been neglected. We focus our attention on the special case $J_a = J_b \equiv J$ in which the technicalities of the diagonalization scheme are not excessive and the ground-state properties are easily evidenced. The general case $J_a \neq J_b$ will be discussed elsewhere. The diagonalization process is effected in two steps. First, by exploiting the unitary transformation $\hat{U} = \exp(i\phi\hat{L})$ with $\hat{L} = i(\hat{\alpha}\hat{\beta}^\dagger - \hat{\beta}\hat{\alpha}^\dagger)$, which generates the mode transformations

$$\begin{cases} \hat{U}^\dagger (\hat{\alpha} + \hat{\alpha}^\dagger) \hat{U} = (\hat{\alpha} + \hat{\alpha}^\dagger) \cos(\phi) + (\hat{\beta} + \hat{\beta}^\dagger) \sin(\phi), \\ \hat{U}^\dagger (\hat{\beta} + \hat{\beta}^\dagger) \hat{U} = (\hat{\beta} + \hat{\beta}^\dagger) \cos(\phi) - (\hat{\alpha} + \hat{\alpha}^\dagger) \sin(\phi). \end{cases}$$

For ϕ such that $\text{tg}(2\phi) = 2W\sqrt{N_a N_b}/(U_b N_b - U_a N_a)$ (obtained by requiring that the term coupling modes α and β vanishes in the new Hamiltonian), these transformations supply the mode-decoupled formula $\hat{H}_{dec} = \hat{U} \hat{H} \hat{U}^\dagger$, whose explicit expression is

$$\begin{aligned} \hat{H}_{dec} = & K - 2J + \left(J + \frac{u - D}{8} \right) (2N_\alpha + 1) + \frac{u - D}{8} (\alpha^{\dagger 2} + \alpha^2) \\ & + \left(J + \frac{u + D}{8} \right) (2N_\beta + 1) + \frac{u + D}{8} (\beta^{\dagger 2} + \beta^2), \end{aligned} \quad (\text{A.2})$$

in which

$$D = \sqrt{\Delta^2 + 4W^2 N_a N_b}, \quad u = U_a N_a + U_b N_b, \quad \Delta = U_a N_a - U_b N_b.$$

We have tacitly assumed $U_b N_b > U_a N_a$ in $\text{tg}(2\phi)$. Note that, if $U_b N_b < U_a N_a$, the angle ϕ will be negative and the definitions of R_α , R_β simply exchange with each other.

The second step follows from the observation that the two subHamiltonians for modes α and β are linear combinations of the generators of the two algebras $SU(1,1)$ $\hat{K}_3^\sigma = (2\hat{\sigma}^\dagger\hat{\sigma} + 1)/4$, $\hat{K}_+^\sigma = \hat{\sigma}^{\dagger 2}/2$ and $\hat{K}_-^\sigma = (\hat{K}_+^\sigma)^\dagger$ where $\hat{\sigma} = \hat{\alpha}, \hat{\beta}$. Then they can be reduced to the diagonal form (see, for example, Ref. [42]) by using the simple $SU(1,1)$ -group transformations $\hat{S}_\sigma = \exp[\theta_\sigma(\hat{K}_+^\sigma - \hat{K}_-^\sigma)/2]$ having the typical form of a squeezing operator. The diagonal Hamiltonian is given by

$$\hat{H}_D = \hat{S}_\alpha^\dagger \hat{S}_\beta^\dagger \hat{H}_{dec} \hat{S}_\beta \hat{S}_\alpha = K - 2J + \sqrt{R_\alpha} (2\hat{N}_\alpha + 1) + \sqrt{R_\beta} (2\hat{N}_\beta + 1),$$

with $R_\alpha = J[J + (u - D)/4]$, $R_\beta = J[J + (u + D)/4]$, when the angles θ_α and θ_β are assumed to satisfy the condition $\text{th}(2\theta_\sigma) = (R_\sigma - J^2)/(R_\sigma + J^2)$ with $\sigma = \alpha, \beta$.

Appendix B. Reduction of \hat{H} to a diagonal form in the regime $|W| > U_c$

Due to $N_{aR} \ll N_a$ and $N_{bL} \ll N_b$, the Bogoliubov approximation reduces \hat{H} to the effective Hamiltonian involving modes \hat{a}_R and \hat{b}_L

$$\hat{H}_1 = C(N_a, N_b) + \sigma_a \hat{N}_{aR} + \sigma_b \hat{N}_{bL} - J_a \sqrt{N_a} (\hat{a}_R^\dagger + \hat{a}_R) - J_b \sqrt{N_b} (\hat{b}_L^\dagger + \hat{b}_L), \quad (\text{B.1})$$

with

$$C(N_a, N_b) = \frac{1}{2} \sum_{c=a,b} U_c (N_c^2 - N_c), \quad \sigma_a = W N_b - U_a N_a, \quad \sigma_b = W N_a - U_b N_b.$$

The opposite case $N_{aL} \ll N_a$ and $N_{bR} \ll N_b$ leads to the effective Hamiltonian

$$\hat{H}_2 = C(N_a, N_b) + \sigma_a \hat{N}_{aL} + \sigma_b \hat{N}_{bR} - J_a \sqrt{N_a} (\hat{a}_L^\dagger + \hat{a}_L) - J_b \sqrt{N_b} (\hat{b}_R^\dagger + \hat{b}_R). \quad (\text{B.2})$$

The eigenstates (17) of \hat{H}_1 include states $|z_{bL}, N_{bL}\rangle = \hat{D}(z_{bL})|N_{bL}\rangle$ and $|z_{aR}, N_{aR}\rangle = \hat{D}(z_{aR})|N_{aR}\rangle$ representing generalized Glauber coherent states. The two unitary transformations (taking \hat{H} into the diagonal form)

$$\hat{D}(z_{aR}) = e^{z_{aR}\hat{a}_R^\dagger - z_{aR}^* \hat{a}_R}, \quad \hat{D}(z_{bL}) = e^{z_{bL}\hat{b}_L^\dagger - z_{bL}^* \hat{b}_L},$$

where

$$z_{aR} = J_a \sqrt{N_a} / \sigma_a, \quad z_{bL} = J_b \sqrt{N_b} / \sigma_b, \quad (\text{B.3})$$

represent displacement operators of the Weyl-Heisenberg groups associated to modes \hat{a}_R and \hat{b}_L . Here, the notation introduced in equation (3) for a generic Fock state $|i, j\rangle_L |N_a - i, N_b - j\rangle_R$ has been replaced by the more effective fully-factorized one: $|N_{aL}\rangle |N_{bL}\rangle |N_{aR}\rangle |N_{bR}\rangle$ where $N_{aL} = i$, $N_{bL} = j$, $N_{aR} = N_a - i$ and $N_{bR} = N_b - j$. Similar to eigenstates (17), the states associated to eigenvalues (18)

$$|E_2(N_{aL}, N_{bR})\rangle = |z_{aL}, N_{aL}\rangle |N_{bL}\rangle |N_{aR}\rangle |z_{bR}, N_{bR}\rangle,$$

with $N_{aR} = N_a - N_{aL}$, $N_{bL} = N_b - N_{bR}$, include two generalized Glauber coherent states defined by $|z_{aL}, N_{aL}\rangle = \hat{D}(z_{aL})|N_{aL}\rangle$ and $|z_{bR}, N_{bR}\rangle = \hat{D}(z_{bR})|N_{bR}\rangle$ where \hat{D} 's represent displacement operators.

Concerning the generalized Glauber state defined by $|z, n\rangle = \hat{D}(z)|n\rangle$, it is worth recalling that their distinctive feature consists in providing the minimum-uncertainty relation $\Delta_x^2 \Delta_p^2 = (2n+1)^2/4$, where the canonical operators \hat{x} and \hat{p} are related to the boson mode $\hat{a} = (\hat{x} + i\hat{p})/\sqrt{2}$, $|n\rangle$ is a number-operator state, and $\hat{D}(z) = \exp(z\hat{a}^\dagger - z^*\hat{a})$.

Appendix C. Diagonal Hamiltonian for $W < 0$

In the attractive case, the Hamiltonians obtained from the Bogoliubov scheme entails the excited states

$$|E_3(N_{aR}, N_{bR})\rangle = |N_{aL}\rangle |N_{bL}\rangle |z_{aR}, N_{aR}\rangle |z_{bR}, N_{bR}\rangle,$$

with $N_{aL} = N_a - N_{aR}$, $N_{bL} = N_b - N_{bR}$, and

$$|E_4(N_{aL}, N_{bL})\rangle = |z_{aL}, N_{aL}\rangle |z_{bL}, N_{bL}\rangle |N_{aR}\rangle |N_{bR}\rangle,$$

with $N_{aR} = N_a - N_{aL}$, $N_{bR} = N_b - N_{bL}$. These provide the lowest-energy state (characterized by the absolute minimum uncertainty) for $N_{aR}, N_{bR} = 0$ and $N_{aL}, N_{bL} = 0$, respectively. The corresponding eigenvalues are easily found to be

$$E_3(N_{aR}, N_{bR}) \simeq \tilde{E}_0(N_a, N_b) + \sigma_a N_{aR} + \sigma_b N_{bR}, \quad (\text{C.1})$$

$$E_4(N_{aL}, N_{bL}) \simeq \tilde{E}_0(N_a, N_b) + \sigma_a N_{aL} + \sigma_b N_{bL}, \quad (\text{C.2})$$

where $\tilde{E}_0(N_a, N_b) = E_0(N_a, N_b) - |W|N_a N_b$ (E_0 is given by Eq. (15)) and the interspecies interaction W has been replaced with $|W|$ in σ_a and σ_b . As for eigenvalues (14) and (18), formulas (C.1) and (C.2) describe the same spectrum.

References

- [1] Kuklov A B, and Svistunov B 2003 *Phys. Rev. Lett.* **90** 100401
- [2] Altman E, Hofstetter W, Demler E and Lukin M D 2003 *New J. Phys.* **5** 113
- [3] Isacsson A, Cha M C, Sengupta K and Girvin S M 2005 *Phys. Rev. B* **72** 184507
- [4] Catani J, De Sarlo L, Barontini G, Minardi F, and Inguscio M 2008 *Phys. Rev. A* **77** 011603(R)
- [5] Gadway B, Pertot D, Reimann R, and Schneble D 2010 *Phys. Rev. Lett.* **105** 045303
- [6] Guglielmino M, Penna V, and Capogrosso-Sansone B 2011 *Phys. Rev. A* **84**, 031603(R)
- [7] Benjamin D and Demler E 2014 *Phys. Rev. A* **89** 033615
- [8] Fisher M P A, Weichman P B, Grinstein G, and Fisher D S, 1989 *Phys. Rev. B* **40** 546
- [9] Jaksch D, Bruder C, Cirac J I, Gardiner C W and Zoller P, 1998 *Phys. Rev. Lett.* **81** 3108
- [10] Albiez M, Gati R, Fölling J, Hunsmann S, Cristiani M and Oberthaler M K 2005 *Phys. Rev. Lett.* **95** 010402
- [11] Barone A and Paternò G 1982 *Physics and Applications of the Josephson effect* (New York: Wiley); Otha H 1977 in *SQUID: Superconducting Quantum Devices and their Applications*, edited by H.D. Hahlbohm and H. Lubbig (Berlin: de Gruyter)
- [12] Ashhab S and Lobo C 2002 *Phys. Rev. A* **66** 013609
- [13] Xu X Q, Lu L H, and Li Y Q 2008 *Phys. Rev. A* **78** 043609
- [14] Satjia I I, Balakrishnan R, Naudus P, Heward J, Edwards M and Clark C W 2009 *Phys. Rev. A* **79** 033616

- [15] Mazzarella G, Moratti M, Salasnich L, Salerno M and Toigo F 2009 *J. Phys. B: At. Mol. Opt. Phys.* **42** 125301
- [16] Juliá-Díaz B, Melé-Messeguer M, Guilleumas M and Polls A, 2009 *Phys. Rev. A* **80** 043622
- [17] Mazzarella G, Malomed B, Salasnich L, Salerno M and Toigo F 2011 *J. Phys. B: At. Mol. Opt. Phys.* **44** 035301
- [18] Zhang D W, Fu L B, Wang Z D, and Zhu S L 2012 *Phys. Rev. A* **85** 043609
- [19] Garcia-March M A, Mazzarella G, Dell’Anna L, Juliá-Díaz B, Salasnich L, and Polls A 2014 *Phys. Rev. A* **89** 063607
- [20] Citro R and Naddeo A 2015 *Eur. Phys. J. Special Topics* **224** 503
- [21] Wang W Y, Cao H, Zhu S L, Liu J, Fu L B 2015 *Laser Phys.* **25** 025501
- [22] Naddeo A and Citro R 2010 *J. Phys. B: At. Mol. Opt. Phys.* **43** 135302
- [23] Ziń P, Oleś B and Sacha K 2011 *Phys. Rev. A* **84** 033614
- [24] Wootters W K 1981 *Phys. Rev. D.* **23** 357; Braunstein S L and Caves C M 1994 *Phys. Rev. Lett.* **72** 3439; Helstrom C W 1976 *Quantum Detection and Estimation Theory* (New York: Academic Press), Holevo A S 1982 *Probabilistic and Statistical Aspect of Quantum Theory* (Amsterdam: North-Holland)
- [25] Pezzé L and Smerzi A 2009 *Phys. Rev. Lett.* **102** 100401
- [26] Pitaevskii L and Stringari S 1999 *Phys. Rev. Lett.* **83** 4237; Pitaevskii L and Stringari S 2001 *Phys. Rev. Lett.* **87** 180402
- [27] Anglin J R, Drummond P and Smerzi A 2001 *Phys. Rev. A* **64** 063605
- [28] Ferrini G, Minguzzi A, Hekking F W 2008 *Phys. Rev. A* **78** 023606(R)
- [29] Bennett C H, Bernstein H J, Popescu S and Schumacher B 1996 *Phys. Rev. A* **53** 2046; Hill S and Wootters W 1997 *Phys. Rev. Lett.* **78** 5022; Amico L, Fazio R, Osterloh A and Vedral V 2008 *Rev. Mod. Phys.* **80** 517; Eisert J, Cramer M and Plenio M B 2010 *Rev. Mod. Phys.* **82** 277
- [30] Penna V 2013 *Phys. Rev. E* **87** 052909
- [31] Penna V and Raffa F A 2014 *Int. J. Quantum Inform.* **12** 1560010
- [32] Felicetti S, Pedernales J S, Egusquiza I L, Romero G, Lamata L, Braak D, and Solano E 2015 *Phys. Rev. A* **92** 033817
- [33] Mazzarella G, Moratti M, Salasnich L and Toigo F 2010 *J. Phys. B: At. Mol. Opt. Phys.* **43** 065303
- [34] Milburn G J, Corney J, Wright E M and Walls D F 1997 *Phys. Rev. A* **55** 4318
- [35] Gilmore R, Bowden C M and Narducci L M 1975 *Phys. Rev. A* **12** 1019
- [36] Buonsante P, Penna V 2008 *J. Phys. A: Math. Gen.* **41** 175301
- [37] Buonsante P, Penna V, Vezzani A 2010 *Phys. Rev. A* **82** 043615
- [38] Mazzarella G, Salasnich L, Parola A and Toigo F 2011 *Phys. Rev. A* **83** 053607
- [39] Lingua F, Guglielmino M, Penna V, and Capogrosso-Sansone B 2015 *Phys. Rev. A* **92**, 053610
- [40] Solomon A I, Feng Y and Penna V 1999 *Phys. Rev. B* **60** 3044
- [41] Landau L D and Lifshits E M 1957 *Quantum Mechanics* (Oxford: Pergamon)
- [42] Cavaletto S M and Penna V 2011 *J. Phys. B: At. Mol. Opt. Phys.* **44** 115308